



1 **Black carbon content of traffic emissions impacts significantly on black carbon**
2 **mass size distributions and mixing states**

3 **Fei Li^{1,3,5#}, Biao Luo^{2,4#}, Miaomiao Zhai^{2,4}, Li Liu³, Gang Zhao⁷, Hanbing Xu⁶, Tao Deng³,**
4 **Xuejiao Deng³, Haobo Tan³, Ye Kuang^{2,4*}, Jun Zhao^{1*}**

5 ¹ School of Atmospheric Sciences, Guangdong Province Key Laboratory for Climate Change and
6 Natural Disaster Studies, and Southern Marine Science and Engineering Guangdong Laboratory
7 (Zhuhai), Sun Yat-sen University, Zhuhai, 519082, China

8 ² Institute for Environmental and Climate Research, Jinan University, Guangzhou, 511443, China.

9 ³ Institute of Tropical and Marine Meteorology, China Meteorological Administration, Guangzhou,
10 510640, China

11 ⁴ Guangdong-Hongkong-Macau Joint Laboratory of Collaborative Innovation for Environmental
12 Quality, Guangzhou, 511443, China.

13 ⁵ Xiamen Key Laboratory of Straits Meteorology, Xiamen Meteorological Bureau, Xiamen, 361012,
14 China

15 ⁶ Experimental Teaching Center, Sun Yat-Sen University, Guangzhou 510275, China

16 ⁷ State Key Joint Laboratory of Environmental Simulation and Pollution Control, International Joint
17 Laboratory for Regional Pollution Control, Ministry of Education, College of Environmental Sciences
18 and Engineering, Peking University, Beijing, 100871, China

19

20 # These authors contribute equally to this paper.

21

22 Corresponding author: Ye Kuang (kuangye@jnu.edu.cn) and Jun Zhao

23 (zhaojun23@mail.sysu.edu.cn)

24

25



26 **Abstract**

27 Both the size and mixing state of black carbon (BC)-containing aerosols are crucial in estimating
28 the environmental, health and climate impacts of BC. Traffic emissions are a major global source of
29 BC, however, parameterization of BC mass size distributions and mixing states associated with traffic
30 remains lacking due to its dependence on vehicle types and driving conditions. To investigate BC mass
31 size distributions and mixing states associated with traffic emissions, a field campaign was conducted
32 in Guangzhou urban area during winter, which used a system coupling a differential mobility analyzer
33 (DMA) and single-particle soot photometer (SP2) to measure BC mass size distributions in the range
34 of 100 to 700 nm. The resolved primary organic aerosols were hydrocarbon-like organic aerosols
35 (HOA) and cooking-like organic aerosols (COA), refractory BC (rBC) which was detected by the
36 DMA-SP2 and correlated highly with HOA ($R^2=0.88$), confirming that traffic emissions are the
37 dominant source of atmospheric BC during the observations. The BC mass size distribution was found
38 to be best fitted by a lognormal distribution, with a geometric mean ($D_{g,BC}$) of 258 ± 16 nm, varying
39 between 200 and 300 nm. During daytime, active formation of secondary nitrate and organic aerosols
40 was observed, but it had little effect on the variations of BC mass size distributions. Further analyses
41 revealed that $D_{g,BC}$ was highly correlated with rBC/HOA ($R=0.66$) in a linear form of $D_{g,BC} =$
42 $34 \times rBC/HOA + 177$, demonstrating that the BC content of traffic emissions significantly impacts the
43 BC mass size distributions. In addition, the size-dependent fractions of BC-containing aerosols in all
44 types of aerosols (f_{BCc}) and the fraction of identified externally mixed (bare/thinly coated) BC particles
45 in all BC-containing aerosols (f_{ext}) were also characterized. It was found that the daytime secondary
46 aerosol formation reduced both f_{BCc} and f_{ext} , with the decrease of f_{ext} being more pronounced for larger
47 particles, possibly due to the higher relative coating thickness. Variations in f_{ext} during nighttime were
48 mainly controlled by the emission conditions. For example, f_{ext} for 600 nm particles decreased from
49 0.82 to 0.46 as rBC/HOA increased from 1 to 3.5 while the mass ratios of secondary aerosols to rBC
50 varied little, demonstrating that the BC content also significantly affects the mixing states of freshly
51 emitted BC from traffic emissions. This study suggests that BC content likely plays a key role in
52 parameterizing both mass size distributions and mixing states of BC from traffic emissions and hence
53 has significant implications for accurate representation of BC from different sources when modeling
54 the impacts of BC.



55 **1 Introduction**

56 Aerosols impact significantly on human health through deposition on human tissues, visibility,
57 weather and climate through interacting with solar radiation and acting as cloud condensation nuclei
58 (CCN). Most of the atmospheric aerosols scatter readily while absorbing negligibly or little solar
59 irradiation, but one exception is black carbon (BC) which absorbs solar irradiation strongly and thus
60 heats the atmosphere. This strong absorption makes BC the second atmospheric warming component
61 (Bond et al., 2013) and plays a major role in climate and air pollution. Menon et al. (2002) found that
62 BC's absorption could affect trends of droughts and floods in India and China by altering regional
63 atmospheric stability and vertical motions. The heating effects of BC in the atmospheric boundary
64 layer can suppress boundary layer turbulence, impacting boundary layer development and meteorology
65 (Wilcox et al., 2016), and consequently affecting local haze formation (Ding et al., 2016). Moreover,
66 BC-containing aerosols can interact with clouds and serve as CCN (Zhang et al., 2017; Motos et al.,
67 2019; Hu et al., 2021), thus indirectly impacting climate (Koch and Del Genio, 2010). These effects of
68 BC can be quantitatively determined through its radiative forcing. In addition, inhalation of
69 atmospheric BC also poses a threat to human health; evidence suggests that it may be associated with
70 changes in subclinical cardiovascular health effects in individuals (Nichols et al., 2013).

71 The radiative and health effects of BC are highly dependent on its size and mixing state, as these
72 factors determine the distribution of BC in aerosols and their optical properties (Bond et al., 2006),
73 hygroscopic growth (Liu et al., 2013), and depositions in the human respiratory tract (Man et al., 2022).
74 Freshly emitted BC can be either almost bare or coated with other materials, usually organic aerosols,
75 which can then undergo rapid aging processes through vapor condensation or serving as medium for
76 reactions (Zhang et al., 2018a; Zhang et al., 2020a; Zhang et al., 2021). This leads to size and
77 morphological changes of BC-containing aerosols (Zhang et al., 2008) and influences their physical
78 properties, such as hygroscopicity (Liu et al., 2013) and activation abilities (Ding et al., 2019; Yu et al.,
79 2022). The coating of other components on BC can also significantly affect the optical properties of
80 BC-containing aerosols, such as the lensing effect that enhances light absorption (Bond et al.,
81 2006; Peng et al., 2016). This effect is non-linear (Liu et al., 2017; Wang et al., 2021) and is highly
82 dependent on the mixing state heterogeneity of BC-containing aerosols (Fierce et al., 2020; Zhao et al.,
83 2021; Zhai et al., 2022a). In addition, Zhao et al. (2019) showed that the BC mass size distributions



84 also play a major role in the direct radiative effects of BC. The size and mixing states of BC, as well
85 as the chemical composition of its coatings, vary significantly with sources (Zhang et al., 2020b). This
86 results in marked differences in the aging processes of freshly emitted BC from different sources in
87 the atmosphere, depending on the emission sources and meteorological conditions in a given location.

88 Guangzhou is an expansive metropolis in the highly industrialized Pearl River Delta (PRD) region
89 of China. Previous studies have shown that emissions from fossil fuel combustion are major sources
90 of BC (Liu et al., 2014) while biomass burning emissions might also make certain contributions during
91 autumn and winter (Sun et al., 2020). However, recent studies on source apportionment have not
92 detected obvious signals attributed to biomass burning in autumn and winter, suggesting that other
93 sources such as traffic activities are the main contributors to BC emissions (Guo et al., 2020; Chen et
94 al., 2021b; Liu et al., 2022; Zhai et al., 2022b). Few studies have used the single-particle soot
95 photometer (SP2) to measure bulk BC mass concentrations and mixing states in Guangzhou urban area
96 (Huang et al., 2011; Tao et al., 2021). Furthermore, no comprehensive measurements that characterize
97 both size distribution and mixing states of BC in this region have been conducted, and the factors that
98 control variations in BC mass size distributions and mixing states remain unknown. BC emissions
99 from diesel vehicles dominate traffic BC emissions (Bond et al., 2013) and depend on many factors,
100 such as fuel type, engine operating conditions, engine types, driving patterns, and environmental
101 conditions (Adler et al., 2010). These conditions have a significant impact on the size distributions and
102 mixing states of emitted particles (Lähde et al., 2011; Xu et al., 2014), therefore BC mass size
103 distributions and mixing states vary a lot in real traffic conditions. While numerous studies have
104 examined the BC size and mixing states of emissions from various types of vehicles (Adler et al.,
105 2010; Liu et al., 2017), only a few have directly investigated the BC size distribution and mixing states
106 as a function of aerosol mobility diameter using the DMA-SP2 system which couples differential
107 mobility analyzer (DMA) and SP2 (Raatikainen et al. (2017), and reported the average coating
108 characteristics of aerosol particles emitted from diesel vehicle exhaust (Han et al., 2019; Zhang et al.,
109 2020b). However, the variations of BC mass size distributions and BC mixing states from real traffic
110 emissions using the DMA-SP2 system have rarely been studied, and how to parameterize them remains
111 elusive. This study carried out a field campaign and employed the DMA-SP2 system to investigate the
112 dominant contribution of traffic emissions to atmospheric BC, which provided an ideal opportunity to
113 evaluate how primary traffic emissions and their subsequent aging can affect BC mass size



114 distributions and mixing states.

115 **2 Materials and Methods**

116 **2.1 Campaign information**

117 The campaign was conducted to characterize BC mass size distributions and mixing states from
118 11 January to 27 February 2022 at the Haizhu wetland park in Guangzhou. The instruments used for
119 characterizing aerosol chemical and physical properties included a quadrupole aerosol chemical
120 speciation monitor (Q-ACSM) for monitoring aerosol chemical compositions, a DMA-SP2 system for
121 measuring BC mass size distributions and mixing states, and a scanning mobility particle sizer (SMPS)
122 system for measuring aerosol particle number size distributions ranging from 13 nm to 800 nm. An
123 AE33 aethalometer (Drinovec et al., 2015) was used to measure aerosol absorptions at multiple
124 wavelengths and indirectly measure bulk BC mass concentrations. A PM_{2.5} inlet (BGI, SCC 2.354)
125 with a flow rate of 8 L/min was used for aerosol sampling. The flow rates of the Q-ACSM, CPC, SP2
126 and AE33 instruments were set to 3 L/min, 0.3 L/min, 0.1 L/min, and 5 L/min, respectively, to meet
127 the flow rate requirement of the impactor although there are some deviations. All instruments were
128 housed in a temperature-controlled container (23-27 °C) and placed downstream of a Nafion drier
129 designed to lower the sample RH to less than 35% (placed outside of the container and vertically to
130 ensure a straight line of the sampling route so that sampling loss of aerosols can be minimized).
131 Meteorological parameters such as temperature, wind speed and direction, and relative humidity (RH)
132 were measured using an automatic weather station. Further details about this site can be found in Liu
133 et al. (2022).

134 **2.2 DMA-SP2 system and data processing**

135 The SP2 (Droplet Measurement Technologies) can measure aerosol scattering and incandescence
136 signals of individual particles and identify if they contain detectable BC mass. It can also provide BC
137 mass concentrations at the single particle level, thus allowing for the determination of BC mixing states.
138 The scattering signals can be used to estimate the particle size of each BC-free particle; however, a
139 leading-edge-only method is required for sizing BC-containing particles (Schwarz et al., 2006), with
140 the estimated optical-equivalent size potentially deviating substantially from the mobility size due to
141 variations in aerosol refractive index and morphology. As such, the use of the DMA-SP2 system to
142 measure BC mass size distributions and mixing states has been previously proposed (Raatikainen et



143 al., 2017; Han et al., 2019; Sarangi et al., 2020; Zhao et al., 2021), which complement the size
 144 measurements and additional size information can be used to derive physical properties such as
 145 morphology and effective densities (Zhang et al., 2018b; Wu et al., 2019). A similar system has also
 146 been used for other applications, such as investigation of the hygroscopic properties of BC-containing
 147 aerosols (McMeeking et al., 2011; Liu et al., 2013). The DMA-SP2 set-up of Zhao et al. (2021)
 148 employed a continuous scanning mode of the DMA, allowing for black carbon mass size distribution
 149 (BCMSD) measurements with a time resolution of 5 minutes. However, accurate matching of the time
 150 of particles in the DMA and SP2 is necessary. Some previous studies passed size-selected
 151 monodisperse aerosols to the SP2 at only a few diameters (Zhang et al., 2018b; Han et al., 2019),

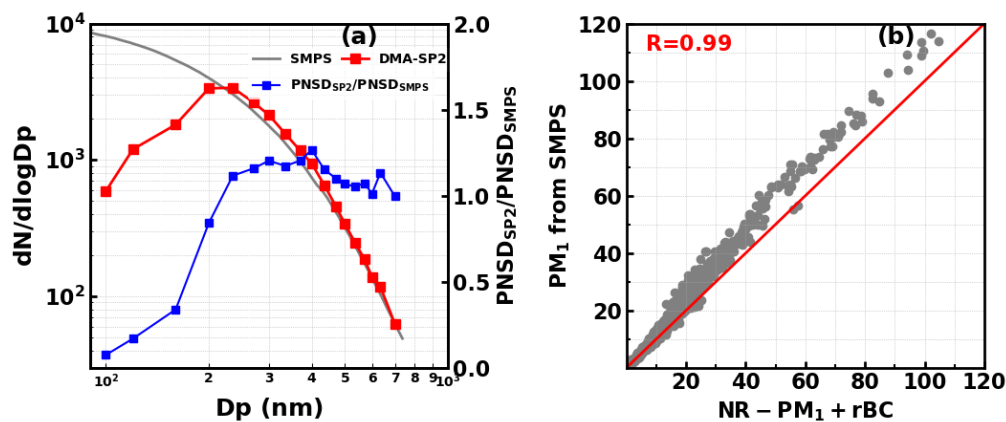


Figure 1. (a) Comparisons between average PNSD observed by the SMPS and inverted from the DMA-SP2 system; (b) Comparison between NR-PM₁+rBC and PM₁ mass concentrations calculated from SMPS measurements.

152 limiting the retrieval of BC mass size distributions and mixing states across the entire submicron
 153 diameter range. In this study, we developed a software which enables the DMA to scan at different
 154 diameters for different time periods depending on their number concentrations. For example, DMA
 155 scans at 100 nm last about 36 seconds, while scans at 700 nm last about 1.5 minutes, allowing for
 156 enough particles to be sampled at larger particle sizes. The diameter set points (18 points) of DMA
 157 scans are 100 nm, 120 nm, 160 nm, 200 nm, 235 nm, 270 nm, 300 nm, 335 nm, 370 nm, 400 nm, 435
 158 nm, 470 nm, 500 nm, 535 nm, 570 nm, 600 nm, 635 nm, and 700 nm, with a full scan taking 20 minutes.

159 With this set-up, the particle number size distributions of BC-containing and BC-free aerosols
 160 can be derived from the DMA-SP2 measurements using an inversion routine that mainly accounts for
 161 the effects of the DMA transfer function and multiple charge. Assuming a BC density of 1.8 g/cm³,



162 the BC volume equivalent diameter of each BC-containing particle (termed as BC core diameter, D_c)
163 can be calculated, assuming a core-shell structure. The particle number size distribution of BC-
164 containing aerosol, containing information of BC mixing states, can then be described using a two-
165 variable formulation $\frac{\partial N}{\partial \log(Dp)\partial \log(Dc)}$, and the multiple charge correction method proposed by Zhao et
166 al. (2021) was used here to account for the impacts of multiple charge on $\frac{\partial N}{\partial \log(Dp)\partial \log(Dc)}$ derivations.
167 Using the derived $\frac{\partial N}{\partial \log(Dp)\partial \log(Dc)}$, the BC mass size distribution with multiple charge corrections
168 accounted for can be derived through integrating rBC mass of each D_c . Details about the inversion
169 routines are introduced in Sect. S1 of the supplement. Note that the effective density of bare BC or
170 BC contained in a particle can vary substantially due to BC morphology and existence of air voids
171 (Zhang et al., 2016; Zhao et al., 2020a). Therefore, a simple assumption of 1.8 g/cm^3 for BC density
172 could bring uncertainties to D_c calculations. In addition, the optical equivalent diameter of BC-
173 containing aerosols cannot be retrieved in this study due to the failure of the SP2 split channel hardware
174 during the campaign, which rendered the leading-edge-only method unusable.

175 The average particle number size distribution (PNSD) derived from the DMA-SP2 system was
176 compared with the one obtained from independent SMPS measurements, as shown in Fig. 1a. The
177 detection limitations of the SP2 scattering channels (Raatikainen et al., 2017) caused the PNSD from
178 SP2 to be markedly lower than that from SMPS for diameters $<200 \text{ nm}$. For diameters larger than 200
179 nm , the PNSD from SP2 was generally consistent with that from SMPS, with the average ratio of
180 SMPS to SP2 measurements being 0.89 ± 0.05 , which is similar to the phenomenon reported in
181 Raatikainen et al. (2017), with an average ratio of 0.82 . Additionally, the observed rBC mass
182 concentrations correlated highly with the optically equivalent BC mass concentrations reported by the
183 AE33 aethalometer ($R^2=0.96$, and an average ratio of 0.96), as shown in Fig. S4. The consistency tests
184 between the DMA-SP2 system and SMPS measurements validated the number size distributions and
185 BC mass concentrations inverted from DMA-SP2 measurements.

186 The number fractions of BC-containing aerosols of various diameters can be calculated using the
187 DMA-SP2 measurements. Based on the time lag between the peak time of the scattering and the
188 incandescence signal (Schwarz et al., 2006; Moteki and Kondo, 2007; Sedlacek Iii et al., 2012), these
189 aerosols can be roughly divided into two categories: bare/thinly coated BC particles and thickly coated
190 BC particles. The time lag distribution of pure BC aerosols can be identified from the SP2 calibrations



191 using bare BC aerosols. Consequently, bare/thinly coated BC particles can be identified using the
192 calibrated critical lag-time.

193 **2.3 Q-ACSM measurements and positive matrix factorization (PMF) analysis**

194 The Q-ACSM measured non-refractory sub-micrometer (NR-PM₁) species, including organic
195 aerosol (OA), sulfate (SO₄), nitrate (NO₃), ammonium (NH₄), and chloride (Cl), at a time resolution
196 of 15 minutes. More detailed description can be referred to Liu et al. (2022) and Ng et al. (2011). The
197 mass spectra measured by the Q-ACSM were analyzed using ACSM standard data analysis software
198 (ACSM Local 1.5.10.0 Released July 6, 2015), written in Igor Pro (version 6.37). The composition-
199 dependent collection efficiency (CE) parameterization scheme proposed by Middlebrook et al. (2012)
200 was used to calculate the mass concentrations of OA and inorganic species. This was also detailed in
201 Liu et al. (2022). As calibration of the Q-ACSM was not available during this campaign, relative
202 ionization efficiencies (RIEs) of 5.15 and 0.7 for ammonium and sulfate from previous calibrations
203 were used, while the default RIEs of 1.4, 1.1, and 1.3 were used for organic aerosol, nitrate, and
204 chloride, respectively. The quality assurance of the Q-ACSM measurements was first performed
205 through comparing the mass concentrations of PM₁ (summation of measured NR-PM₁ concentrations
206 and rBC concentrations measured by the DMA-SP2 system) with PM₁ mass concentrations calculated
207 from the particle number size distribution measurements of SMPS, assuming an aerosol density of 1.6
208 g/cm³. Good consistency (as shown in Fig. 1b) was achieved between SMPS and Q-ACSM
209 measurements (R=0.99), with NR-PM₁+rBC values slightly lower than PM₁ concentrations from
210 SMPS (an average ratio of 1.19). Two reasons explain the deviation: 1) the assumed average aerosol
211 density may be biased from the real variations; 2) some aerosol species are not measured by the Q-
212 ACSM, such as sub-micrometer dust.

213 Following the same procedure of the PMF analysis for the Q-ACSM measurements introduced in
214 Liu et al. (2022) and Zhai et al. (2022b), the PMF technique with the multilinear engine (ME-2)
215 (Canonaco et al., 2013; Canonaco et al., 2021) was applied to ACSM spectra for deconvolving OA into
216 different factors and detailed in the supplement. In total, four factors were identified, including two
217 primary OA (POA) factors: a hydrocarbon-like OA (HOA, O/C~0.16) and a cooking-like OA (COA,
218 O/C~0.14); and two oxygenated OA factors: a less oxidized oxygenated OA (LOOA, O/C~0.89) and
219 a more oxidized oxygenated OA (MOOA, O/C~0.94). SOA was represented by the summation of
220 LOOA and MOOA as done in previous studies (Kuang et al., 2020). The mass spectra of these factors,



221 the determination of the factor number, the selection of solutions and more details about the factor
222 analysis can be found in Sect. S2 of the supplement.

223

224 **3 Results and discussion**

225 **3.1 Overview of DMA-SP2 measurements and aerosol chemical composition**

226 During the observation period, the PM_{2.5} mass concentration varied significantly (from 1 to 126
227 µg/m³) with an average of 20 µg/m³ and several pollution episodes were observed during relatively
228 stagnant conditions when wind speeds were near or below 1 m/s. The time series of meteorological
229 parameters as well as PM_{2.5}, ammonium sulfate (AS), ammonium nitrate (AN), SOA, HOA, COA and
230 rBC are shown in Fig. 2. The scheme proposed by Gysel et al. (2007) was used to identify AS and AN.
231 On average, secondary aerosols including nitrate, sulfate, ammonium and SOA together accounted for
232 about 80% of non-refractory PM₁ mass concentration and secondary aerosols increased substantially
233 during pollution episodes, demonstrating active secondary aerosol formations during the observations
234 which might significantly impact BC mass size distributions as well as BC mixing states. The average
235 air RH during the observations varied a lot from 42% to 98% with an average of 76%, suggesting that
236 the heterogeneous reactions that involve aerosol water were favored during this campaign, which is
237 consistent with the quick formation of ammonium nitrate in pollution episodes. On average, AN, AS
238 and SOA accounted for 33%, 25% and 42% of secondary aerosols respectively, which is consistent
239 with Zhai et al. (2022b) that nitrate concentrations are higher than sulfate during winter in Guangzhou
240 urban area, especially under pollution conditions. The time series of rBC mass concentrations were
241 shown in Fig. 2d, with rBC mass concentrations ranging from about 0.1 to 20 µg/m³ with an average
242 of 2.3 µg/m³. Resolved POA factors were HOA and COA, which is consistent with results of previous
243 studies in recent years that traffic emissions and cooking emissions are two main sources of primary
244 aerosols in Guangzhou urban area (Guo et al., 2020; Chen et al., 2021a; Chen et al., 2021b). The rBC



245 correlated highly with HOA ($R^2=0.88$), demonstrating that traffic emissions contributed dominantly to

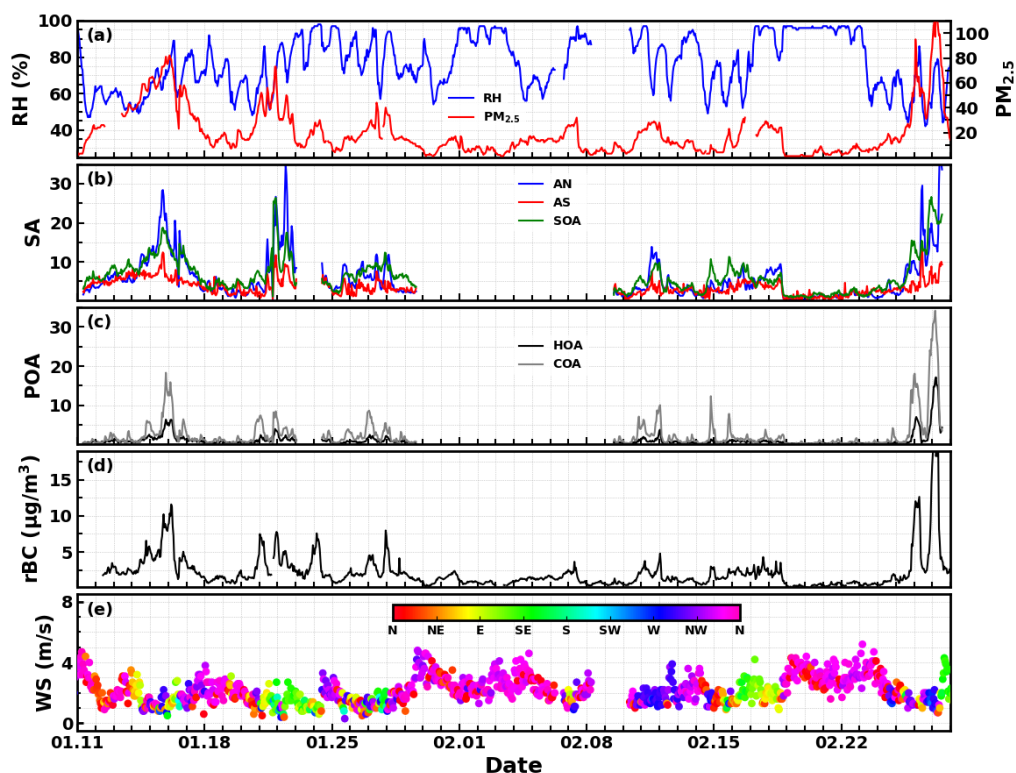


Figure 2. Timeseries of (a) RH and PM_{2.5}; (b) secondary aerosols including nitrate, sulfate and OOA; (c) HOA and COA; (d) rBC; (e) wind speed and directions.

246 atmospheric BC during the observations.

247 The observed average BC mass size distribution, as shown in Fig. 3a, exhibits a single lognormal
248 mode for diameters greater than 100 nm, with a fitted geometric mean ($D_{g,BC}$) of 258 nm ranging from
249 200 nm to 300 nm. The formula form of fitting is introduced in Eq.1 of the supplement, and the mean
250 of fitted geometric standard deviation (σ_g) is 1.69. A small mass mode might exist for diameters less
251 than 100 nm; however, it cannot be characterized due to the detection limitation of the SP2, which
252 measures BC-containing particles with a D_c larger than 80 nm. Previous studies have reported BC mass
253 size distribution as a function of rBC core diameter (Kompalli et al., 2020; Liu et al., 2019). The
254 retrieved $D_{g,BC}$ is higher than most mass median diameters of rBC core measured in urban
255 environments, near 200 nm in urban Beijing (Liu et al. (2019) which is reasonable due to intrinsic
256 coatings (Adler et al., 2010). Some prior studies reported BC mass size distribution as a function of



257 mobility diameter D_p measured by coupling the DMA with aethalometer (Stabile et al., 2012; Ning et al., 2013; Zhao et al., 2019). A few studies also reported BC mass size distribution as a function of
 258 aerodynamic diameter using the size-segregation filtering method (Hu et al., 2012). Zhao et al. (2019)
 259 reported bimodal characteristics of BC mass size distribution in the North China Plain, with the second
 260 mode accounting for most of the rBC mass and a $D_{g,BC}$ of the coarse mode ranging from 430 to 580
 261 nm, which is much higher than the average one reported here. This difference may be attributed to the
 262 markedly different sources of rBC (Zhang et al., 2020b) and the different roles of BC-containing
 263

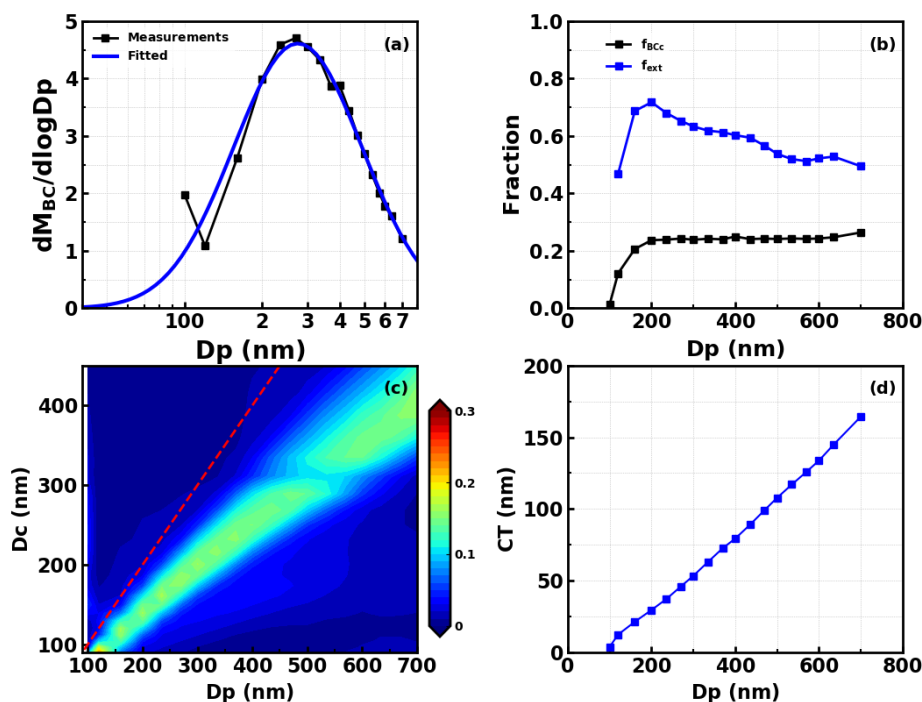


Figure 3. (a) Observed average BCMSD and the lognormal fitting curve; (b) Fractions of identified BC-containing aerosols in all aerosols at different diameters and fractions of externally mixed BC (bare BC) in BC-containing aerosols; (c) Average D_c distributions at different diameters, the red dashed line is the 1:1 line; (d) Average coating thickness (CT).

264 aerosols in the formation of secondary aerosols.

265 The BC mixing state is an essential factor for determining the BC's climate effects. Fig. 3b
 266 displays the average size-dependent fractions of BC-containing aerosols (f_{BC}) and the fraction of
 267 identified externally mixed (bare/thinly coated) BC particles (f_{ext}) in all BC-containing aerosols. For



268 diameters below 200 nm, not all BC-free aerosols were detected by the SP2, so the number
269 concentration of all aerosols from SMPS measurements was used to calculate f_{BCc} . The results show a
270 decrease in f_{BCc} from 200 nm to 100 nm, reaching nearly 0.01 at 100 nm. This may be due to the lower
271 fraction of BC-containing aerosols at smaller diameters, as well as the detection limit (~ 80 nm) of the
272 SP2, which may fail to detect many BC-containing aerosols below 80 nm. This can be further explained
273 based on the measurements from the volatility tandem differential mobility analyzer (V-TDMA) in
274 Guangzhou urban area in previous studies. Cheung et al. (2016) and Tan et al. (2016) used the number
275 fraction of remaining aerosols at 300 °C in V-TDMA measurements to represent f_{BCc} , assuming that
276 all BC-free aerosols had completely evaporated at this temperature. Their results showed an increasing
277 trend in f_{BCc} from 0.62 to 0.86 for diameters ranging from 40 nm to 300 nm, which is much higher than
278 the values reported in this study (ranging from 200 nm to 700 nm, with an average of 0.24). Both
279 methods may be biased in f_{BCc} measurements due to the detection limit of BC mass in the SP2, which
280 may underestimate f_{BCc} (Zhao et al., 2020b), and the assumption that all BC-free aerosols have
281 evaporated at 300 °C in V-TDMA may overestimate f_{BCc} by miscounting some aerosols with extremely
282 low volatility components (Tasoglou et al., 2020). Nevertheless, the low f_{BCc} values obtained from
283 previous V-TDMA measurements confirm that f_{BCc} is smaller for smaller diameters ($D_p < 200$ nm). The
284 size-dependent f_{BCc} is critical for simulating aerosol optical properties (Li et al., 2019) and CCN
285 predictions (Ren et al., 2018). The facts that most BC masses reside in particles larger than 100 nm
286 and most rBC masses would be detected by SP2 suggest that the f_{BCc} reported from SP2 measurements
287 are more suitable for use in aerosol optical simulations. As for f_{ext} , the average f_{ext} shows a decreasing
288 trend from 200 nm to 700 nm, with an average of 0.59, and the f_{ext} at 100 nm being significantly
289 affected by the detection limit. This suggests that BC is generally externally mixed during the
290 observations, with a higher degree of aging for larger particles. The average distributions of rBC core
291 at different diameters are shown in Fig.3c, with a single mode at all diameters, deviating more from
292 the 1:1 line at larger diameters, again indicating a higher degree of aging for larger particles. The
293 estimated average coating thickness (CT) at different diameters is shown in Fig. 3d, with CT increasing
294 from 29 nm at 200 nm to 164 nm at 700 nm, and a relative coating thickness (RCT, D_p/D_c) ranging
295 from 1.27 at 200 nm to 1.88 at 700 nm. The RCT of 200 nm is similar to that of BC-containing aerosols
296 freshly emitted from diesel vehicles (Zhang et al., 2020b), consistent with diesel vehicle emissions
297 being the dominant source of BC traffic emissions (Bond et al., 2013).



298 The average diurnal variations of POA, rBC and secondary aerosol components including SOA,
299 AN and AS are depicted in Fig. 4a. In the morning, rBC and POA (HOA+COA) decrease due to

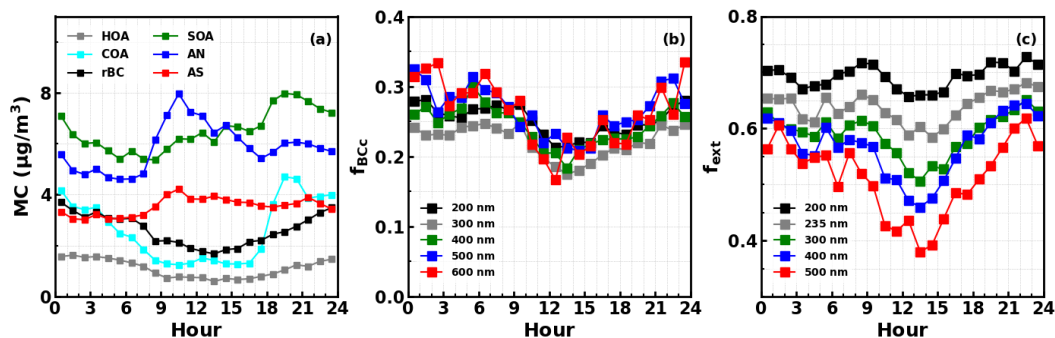


Figure 4. Average diurnal variations of (a) POA, SOA, ammonium nitrate (AN), ammonium sulfate (AS) and rBC ; (b) f_{BCC} at different diameters; (c) f_{ext} at different diameters.

300 dilution effects associated with boundary layer development, whereas SOA concentrations increase
301 since 08:00. However, POA and rBC begin to increase after 14:00, with the diurnal pattern of rBC
302 being generally consistent with that of HOA. The rapid increase in COA after 17:00 does not lead to a
303 significant rise in rBC, confirming that activities associated with cooking contribute negligibly to BC
304 emissions. AN and AS begin to decrease after noon, with SOA continuing to increase until 20:00,
305 which is in line with the findings reported in Zhai et al. (2022b) that the highest SOA mass
306 concentrations result from the coordination of daytime and nighttime SOA formation. The substantial
307 decrease in f_{BCC} was observed in the morning when the prominent SOA formation occur, with the
308 decrease in f_{BCC} being greater as the particle size increases, suggesting that secondary aerosols are
309 formed more efficiently on larger BC-free particles, which are then migrated to larger sizes. This is
310 further supported by the diurnal variations of f_{ext} , which revealed that secondary aerosol formation is
311 more efficient in larger BC-containing aerosols (Fig. 4c). A decrease in f_{ext} from the morning to the
312 afternoon was most prominent for aerosols at 500 nm (0.17), while a small decrease in f_{ext} (0.05) was
313 observed at 200 nm. This is consistent with the findings from the coating thickness results in Fig. 3d,
314 which showed that larger particles have higher coating thickness, and are therefore likely to contain
315 more aerosol water, thus favoring secondary aerosol formation via multiphase reactions.

316



317 **3.2 Impacts of primary emissions and secondary aerosol formation on BC mass size distributions**

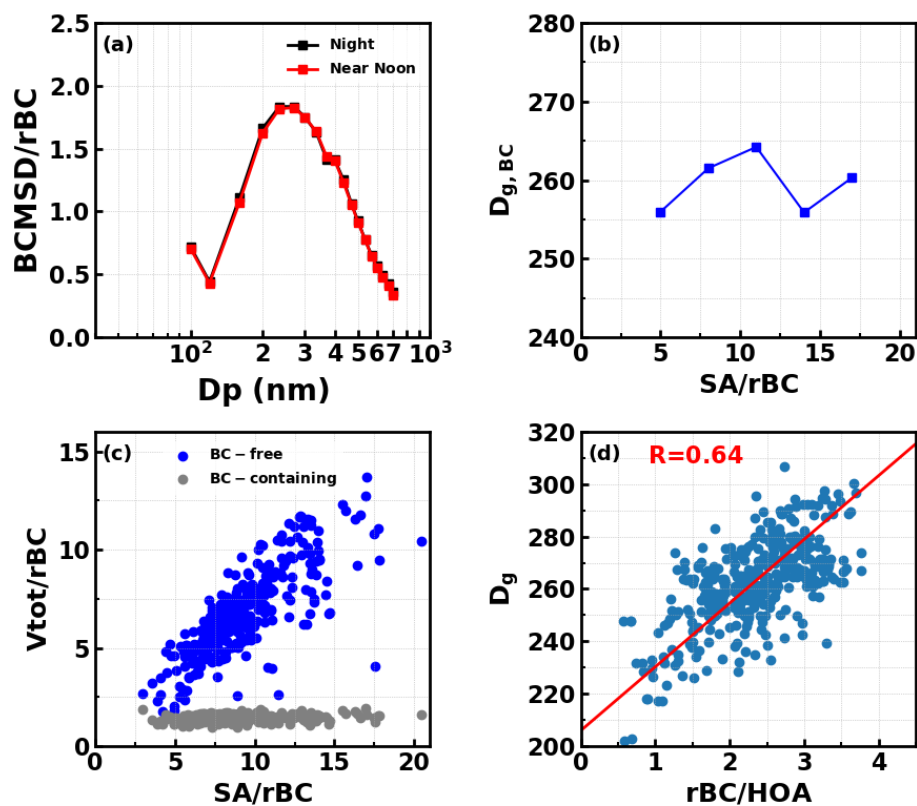


Figure 5. (a) Normalized average BCMSD during night and daytime; (b) Variations of $D_{g,BC}$ as a function of the ratio SA/rBC; (c) Scatter plots of SA/rBC and the ratio total volume (V_{tot}) to rBC of BC free and BC containing aerosols; (d) Correlations between D_g and SA/rBC variations during night.

318 The diurnal variations of f_{ext} revealed that secondary aerosols are formed on BC-containing
319 aerosols, thus impacting mixing states, and this might also result in changes in BC mass size
320 distribution. The average BC mass size distributions are shown in Fig. 5a, which are normalized with
321 rBC during the night (from local time 20:00 to 06:00 the next morning) and during afternoon when
322 active secondary aerosol formation is at its final stage and the impacts of accumulations of primary
323 emissions are relatively small (local time 12:00 to 17:00). Fig.5a indicates that daytime secondary
324 aerosol formation does not modify the shape of BC mass size distributions, which is confirmed by the
325 variations of $D_{g,BC}$ as a function of SA/rBC ratio shown in Fig. 5b (where SA includes mass
326 concentrations of sulfate, nitrate, ammonium and SOA). The DMA-SP2 measurements distinguish
327 BC-free and BC-containing aerosols, allowing for the volume variations of BC-free and BC-containing



328 aerosols with contributions of secondary aerosol formation to be differentiated. As seen in Fig. 5c, as
329 SA/rBC increases, the total volume of BC-containing aerosols increases very slightly, while secondary
330 aerosol formation mainly adds mass to BC-free aerosols, explaining the same BC mass size distribution
331 shape during both daytime and nighttime. Many previous studies have demonstrated that BC can serve
332 as sites for heterogenous reactions (Khalizov et al., 2010) and may even promote secondary aerosol
333 formation, thereby playing a significant role in haze formation (Zhang et al., 2020a). Results from
334 Zhang et al. (2021) pointed out that BC promotes sulfate formation in the urban area of Guangzhou
335 during summer. Our results indicate that BC plays a minor role in haze formation in Guangzhou during
336 winter, which might have significant implications for haze formation mechanisms in this region.

337 The BC primary emissions and their subsequent aging in the air determine the observed BC mass
338 size distributions. The aforementioned little influences of secondary aerosol formation on BC mass
339 size distribution evolution suggest that primary emissions played a significant role in the observed
340 variations in the BC mass size distributions. Traffic emissions dominate BC emissions during the
341 observations as discussed before, and diesel vehicles contribute dominantly to BC emissions from
342 traffic activities (Bond et al., 2013). The results from previous studies indicate that the ratio of
343 elemental carbon (EC) to organic carbon (OC) changed significantly depending on the external factors
344 (Adler et al., 2010; Lu et al., 2012), such as vehicle type, engine load, and driving conditions, etc. This
345 ratio represents the emission conditions of diesel vehicles, which also influences the size distributions
346 of diesel exhaust particles (Lähde et al., 2011; Han et al., 2019). Here, we use the ratio rBC/HOA to
347 represent different emission conditions related to traffic activities and investigate the potential effects
348 of rBC/HOA variations on BC mass size distributions. To avoid the potential effects of secondary
349 aerosol formation and daytime evaporation of HOA due to dilution, only data points from nighttime
350 (from 18:00 to 06:00 the next morning) are used, the results of which are displayed in Fig. 5d. Our
351 results showed for the first time that variations of $D_{g,BC}$ are strongly correlated with rBC/HOA, and a
352 linear relationship of $D_{g,BC} = 34 \times rBC/HOA + 177$ can be derived, indicating that a larger particle
353 diameter of BC-containing aerosols is associated with a higher BC content. Even though rBC and HOA
354 during nighttime in this study are accumulated from different vehicle sources, the relationship between
355 $D_{g,BC}$ and rBC/HOA still holds, suggesting that the black carbon content might be used for
356 parametrizing BC mass size distributions in traffic-related emissions.

357



358 3.3 Impacts of primary emissions and secondary aerosol formation on BC mixing states

359 As introduced in Sect. 3.1, both f_{BCc} and f_{ext} decreased during daytime due to secondary aerosol
 360 formation. Here, the variations of daytime (from 08:00 to 18:00) f_{BCc} and f_{ext} under different SA/rBC
 361 conditions were directly investigated and shown in Fig. 6. The f_{BCc} values ranging from 200 nm to 600
 362 nm decreased from about 0.3 to around 0.175 as SA/rBC increased from 5 to 15 (Fig. 6a), highlighting
 363 significant impacts of secondary aerosol formation on f_{BCc} . As discussed in Sect. 3.1, the decrease of
 364 f_{BCc} should be associated with the fact that secondary aerosols are formed much more quickly on BC-
 365 free aerosols than on BC-containing aerosols, which is consistent with the conclusion in Sect. 3.2 that
 366 secondary aerosol formation mainly adds mass to BC-containing aerosols. New particle formation also
 367 increases the number concentration of BC-free aerosols; however, its impact is limited for aerosol
 368 particles beyond 200 nm (Zhang et al., 2012). The evolution of particle number size distribution shape
 369 beyond 200 nm is mainly associated with vapor condensation, although coagulation also play a role
 370 (Seinfeld and Pandis, 2016).

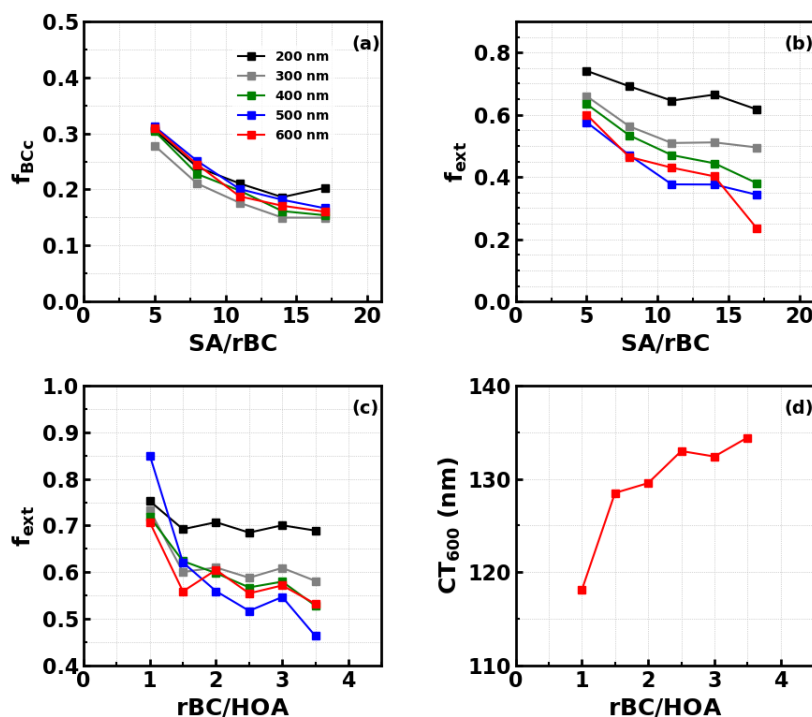


Figure 6. Variations of f_{BCc} (a) and (b) f_{ext} under different SA/rBC conditions; Variations of f_{ext} (c) and coating thickness of aerosols with diameter of 600 nm (d) under different rBC/HOA conditions.



371 The variations in f_{ext} under different SA/rBC conditions are presented in Fig. 6b. Larger particles
372 exhibited a more significant decrease in f_{ext} with SA/rBC increasing from 5 to 17.5, for example, f_{ext}
373 of 200 nm particles only decreased from 0.75 to 0.6, while that of 600 nm particles decreased from 0.6
374 to 0.24. Aside from secondary aerosol formation, the emission conditions are also important factors
375 that influence BC mixing states, particularly due to the contribution of the co-emitted intrinsic organic
376 aerosols (Adler et al., 2010). At night, the shallow boundary layer facilitates the accumulation of
377 freshly emitted aerosols, leading to increases in the mass concentrations of rBC and POA (Fig. 4a) and
378 the mixing of freshly emitted and aged aerosols. Even so, the variations of f_{ext} during night under
379 different rBC/HOA conditions might shed some lights on the impacts of primary emissions on BC
380 mixing states, which is shown in Fig.6c. As rBC/HOA increased from 1 to 3.5, f_{ext} generally decreased,
381 especially for particles larger than 300 nm. The f_{ext} of 600 nm decreased from 0.82 to 0.46, which is
382 higher than the degree of variations influenced by secondary aerosol formation as shown in Fig. 6b,
383 and most importantly SA/rBC decreased from 9.4 to 6.9 as rBC/HOA increased from 1 to 3.5,
384 demonstrating that the change of emission conditions has dominated the nighttime variations of BC
385 mixing states. The increased internal mixing degree of BC observed under higher rBC/HOA conditions
386 is also reflected in the variations of the average coating thickness of BC-containing aerosols. As seen
387 in Fig. 6d, the coating thickness of 600 nm BC-containing aerosols increased from 118 nm to 134 nm
388 as rBC/HOA increased from 1 to 3.5. Interestingly, as rBC/HOA increases, the relative amount of
389 coating to rBC becomes less, however, both fractions of internally mixed BC and coating thickness
390 increase, suggesting that a higher fraction of co-emitted intrinsic OA resides in BC-containing aerosols.
391 This section demonstrates the significant impacts of emission conditions of traffic sources on BC
392 mixing states.

393 **4. Atmospheric implications**

394 The evidence that the secondary aerosol formation mainly adds mass to BC-free particles suggests
395 that reactions occurring on or within BC-containing particles play a limited role in the formation of
396 haze in winter of Guangzhou. The urban area in Guangzhou is quite representative of most urban
397 regions where traffic emissions are the primary source of BC emissions. Hence, the above finding has
398 important implications for the haze formation mechanisms, particularly in Southern China where
399 primary aerosol emissions and meteorological conditions are similar to those in Guangzhou. The size
400 and mixing states of BC-containing particles determine their optical and hygroscopic properties, and



401 are therefore critical factors for evaluating the environmental, health, and climate effects of BC;
402 however, these factors are not adequately considered in both chemical transport and climate models
403 (Bond et al., 2013; Saleh, 2020). The finding that secondary aerosol formation has little effect on the
404 BC mass size distribution suggests that the study provides an excellent case scenario to investigate
405 how changes in traffic emissions affect the BC mass size distribution and mixing states. It further
406 shows that BC content in traffic emissions has a significant impact on both the BC mass size
407 distribution and mixing states, and the almost linear trends between $D_{g,BC}$ and r_{BC}/HOA suggest that
408 BC content can be used as the key factor to parameterize both the BC mass size distribution and mixing
409 states from traffic emissions, which warrants future comprehensive investigation.

410 Traffic is a major global contributor to atmospheric BC concentrations, but other major sources,
411 such as biomass burning and coal combustion, as well as off-road diesel engines, also contribute
412 significantly to BC emissions and play an even more important role than traffic in some regions (Bond
413 et al., 2013). It is hence also important to investigate whether BC content of other major BC sources
414 than traffic are important in determining BC mass size distributions and mixing states. Saleh et al.
415 (2014) found that BC content has a major effect on the brownness of organic aerosols emitted from
416 biomass burning, and results from several later studies further confirmed this finding (Luo et al., 2022).
417 Recently, Saleh (2020a) discussed the potential for parameterizing the optical properties of brown
418 carbon using BC content in climate models. Moreover, the results of Luo et al. (2022) demonstrated
419 that BC content can also be used to parameterize the volume size distributions of aerosols emitted from
420 biomass burning, indicating that BC content plays an important role in both traffic emissions and
421 biomass burning emissions. These findings suggest that more comprehensive experiments should be
422 designed in the future to investigate the factors that control variations in BC mass size distributions
423 and mixing states, and to discuss how to use BC content from different major BC sources for
424 parameterizing BC mass size distributions and mixing states.

425

426

427

428

429

430



431 **Data availability.** All data needed are presented in time series of Figures and supplementary Figures,
432 raw datasets of this study are available from the corresponding author Ye Kuang (kuangye@jnu.edu.cn)
433 upon request.

434

435 **Competing interests.** The authors declare that they have no conflict of interest.

436

437 **Author Contributions.** YK and LL planned this campaign, with YK conceived and led this research.
438 FL performed the data analysis and wrote the manuscript together with YK. BL made the DMA-SP2,
439 SMPS and AE33 measurements together with FL and performed the post-processing of the SP2 data
440 with help of GZ, MMZ maintained the Q-ACSM during the observations and performed the PMF
441 analysis. JZ performed fund acquisition and supervision. TD, XJD and HBT helped the data acquisition
442 and revised the manuscript. All authors reviewed and edited the manuscript.

443

444

445 **Acknowledgments**

446 This work is supported by the Guangdong Major Project of Basic and Applied Basic Research (Grant
447 No. 2020B0301030004); Natural Science Foundation of Fujian Province (2021J01463); National
448 Natural Science Foundation of China (42175083 and 42105092); Guangdong Provincial Key Research
449 and Development Program (2020B1111360003); Guangdong Basic and Applied Basic Research
450 Foundation (2019A1515110791); The Special Fund Project for Science and Technology Innovation
451 Strategy of Guangdong Province (Grant No.2019B121205004).

452

453

454



455 References

- 456 Adler, G., Riziq, A. A., Erlick, C., and Rudich, Y.: Effect of intrinsic organic carbon on the optical properties of fresh diesel
457 soot, *Proceedings of the National Academy of Sciences*, 107, 6699-6704, 10.1073/pnas.0903311106, 2010.
- 458 Bond, T. C., Habib, G., and Bergstrom, R. W.: Limitations in the enhancement of visible light absorption due to mixing state,
459 *Journal of Geophysical Research: Atmospheres*, 111, <https://doi.org/10.1029/2006JD007315>, 2006.
- 460 Bond, T. C., Doherty, S. J., Fahey, D. W., Forster, P. M., Berntsen, T., DeAngelo, B. J., Flanner, M. G., Ghan, S., Kärcher, B.,
461 Koch, D., Kinne, S., Kondo, Y., Quinn, P. K., Sarofim, M. C., Schultz, M. G., Schulz, M., Venkataraman, C., Zhang, H., Zhang,
462 S., Bellouin, N., Guttikunda, S. K., Hopke, P. K., Jacobson, M. Z., Kaiser, J. W., Klimont, Z., Lohmann, U., Schwarz, J. P.,
463 Shindell, D., Storelvmo, T., Warren, S. G., and Zender, C. S.: Bounding the role of black carbon in the climate system: A
464 scientific assessment, *Journal of Geophysical Research: Atmospheres*, 118, 5380-5552,
465 <https://doi.org/10.1002/jgrd.50171>, 2013.
- 466 Canonaco, F., Crippa, M., Slowik, J. G., Baltensperger, U., and Prévôt, A. S. H.: SoFi, an IGOR-based interface for the efficient
467 use of the generalized multilinear engine (ME-2) for the source apportionment: ME-2 application to aerosol mass
468 spectrometer data, *Atmos. Meas. Tech.*, 6, 3649-3661, 10.5194/amt-6-3649-2013, 2013.
- 469 Canonaco, F., Tobler, A., Chen, G., Sosedova, Y., Slowik, J. G., Bozzetti, C., Daellenbach, K. R., El Haddad, I., Crippa, M.,
470 Huang, R. J., Furger, M., Baltensperger, U., and Prévôt, A. S. H.: A new method for long-term source apportionment with
471 time-dependent factor profiles and uncertainty assessment using SoFi Pro: application to 1 year of organic aerosol data,
472 *Atmos. Meas. Tech.*, 14, 923-943, 10.5194/amt-14-923-2021, 2021.
- 473 Chen, C., Tan, H., Hong, Y., Yin, C., Deng, X., Chen, B., Wu, M., Bu, Q., Weng, J., and Gan, Q.: Characteristics, formation
474 mechanisms, and sources of non-refractory submicron aerosols in Guangzhou, China, *Atmospheric Environment*, 118255,
475 <https://doi.org/10.1016/j.atmosenv.2021.118255>, 2021a.
- 476 Chen, W., Ye, Y., Hu, W., Zhou, H., Pan, T., Wang, Y., Song, W., Song, Q., Ye, C., Wang, C., Wang, B., Huang, S., Yuan, B., Zhu,
477 M., Lian, X., Zhang, G., Bi, X., Jiang, F., Liu, J., Canonaco, F., Prevot, A. S. H., Shao, M., and Wang, X.: Real-Time
478 Characterization of Aerosol Compositions, Sources, and Aging Processes in Guangzhou During PRIDE-GBA 2018 Campaign,
479 *Journal of Geophysical Research: Atmospheres*, 126, e2021JD035114, <https://doi.org/10.1029/2021JD035114>, 2021b.
- 480 Cheung, H. H. Y., Tan, H., Xu, H., Li, F., Wu, C., Yu, J. Z., and Chan, C. K.: Measurements of non-volatile aerosols with a
481 VTDMA and their correlations with carbonaceous aerosols in Guangzhou, China, *Atmos. Chem. Phys.*, 16, 8431-8446,
482 10.5194/acp-16-8431-2016, 2016.
- 483 Ding, A. J., Huang, X., Nie, W., Sun, J. N., Kerminen, V.-M., Petäjä, T., Su, H., Cheng, Y. F., Yang, X.-Q., Wang, M. H., Chi, X.
484 G., Wang, J. P., Virkkula, A., Guo, W. D., Yuan, J., Wang, S. Y., Zhang, R. J., Wu, Y. F., Song, Y., Zhu, T., Zilitinkevich, S., Kulmala,
485 M., and Fu, C. B.: Enhanced haze pollution by black carbon in megacities in China, *Geophysical Research Letters*, 43, 2873-
486 2879, 10.1002/2016gl067745, 2016.
- 487 Ding, S., Liu, D., Zhao, D., Hu, K., Tian, P., Zhou, W., Huang, M., Yang, Y., Wang, F., Sheng, J., Liu, Q., Kong, S., Cui, P., Huang,
488 Y., He, H., Coe, H., and Ding, D.: Size-Related Physical Properties of Black Carbon in the Lower Atmosphere over Beijing
489 and Europe, *Environmental science & technology*, 10.1021/acs.est.9b03722, 2019.
- 490 Drinovec, L., Močnik, G., Zotter, P., Prévôt, A. S. H., Ruckstuhl, C., Coz, E., Rupakheti, M., Sciare, J., Müller, T., Wiedensohler,
491 A., and Hansen, A. D. A.: The "dual-spot" Aethalometer: an improved measurement of aerosol black carbon with real-
492 time loading compensation, *Atmospheric Measurement Techniques*, 8, 1965-1979, 10.5194/amt-8-1965-2015, 2015.
- 493 Fierce, L., Onasch, T. B., Cappa, C. D., Mazzoleni, C., China, S., Bhandari, J., Davidovits, P., Fischer, D. A., Helgestad, T.,
494 Lambe, A. T., Sedlacek, A. J., 3rd, Smith, G. D., and Wolff, L.: Radiative absorption enhancements by black carbon controlled
495 by particle-to-particle heterogeneity in composition, *Proc Natl Acad Sci U S A*, 117, 5196-5203, 10.1073/pnas.1919723117,
496 2020.
- 497 Guo, J., Zhou, S., Cai, M., Zhao, J., Song, W., Zhao, W., Hu, W., Sun, Y., He, Y., Yang, C., Xu, X., Zhang, Z., Cheng, P., Fan, Q.,



- 498 Hang, J., Fan, S., Wang, X., and Wang, X.: Characterization of submicron particles by time-of-flight aerosol chemical
499 speciation monitor (ToF-ACSM) during wintertime: aerosol composition, sources, and chemical processes in Guangzhou,
500 China, *Atmospheric Chemistry and Physics*, 20, 7595-7615, 10.5194/acp-20-7595-2020, 2020.
- 501 Gysel, M., Crosier, J., Topping, D. O., Whitehead, J. D., Bower, K. N., Cubison, M. J., Williams, P. I., Flynn, M. J., McFiggans,
502 G. B., and Coe, H.: Closure study between chemical composition and hygroscopic growth of aerosol particles during
503 TORCH2, *Atmos. Chem. Phys.*, 7, 6131-6144, 10.5194/acp-7-6131-2007, 2007.
- 504 Han, C., Li, S.-M., Liu, P., and Lee, P.: Size Dependence of the Physical Characteristics of Particles Containing Refractory
505 Black Carbon in Diesel Vehicle Exhaust, *Environmental science & technology*, 53, 137-145, 10.1021/acs.est.8b04603, 2019.
- 506 Hu, D., Liu, D., Kong, S., Zhao, D., Wu, Y., Li, S., Ding, S., Zheng, S., Cheng, Y., Hu, K., Deng, Z., Wu, Y., Tian, P., Liu, Q., Huang,
507 M., and Ding, D.: Direct Quantification of Droplet Activation of Ambient Black Carbon Under Water Supersaturation,
508 *Journal of Geophysical Research: Atmospheres*, 126, e2021JD034649, <https://doi.org/10.1029/2021JD034649>, 2021.
- 509 Hu, M., Peng, J., Sun, K., Yue, D., Guo, S., Wiedensohler, A., and Wu, Z.: Estimation of Size-Resolved Ambient Particle
510 Density Based on the Measurement of Aerosol Number, Mass, and Chemical Size Distributions in the Winter in Beijing,
511 *Environmental science & technology*, 46, 9941-9947, 10.1021/es204073t, 2012.
- 512 Khalizov, A. F., Cruz-Quinones, M., and Zhang, R.: Heterogeneous Reaction of NO₂ on Fresh and Coated Soot Surfaces, *The*
513 *Journal of Physical Chemistry A*, 114, 7516-7524, 10.1021/jp1021938, 2010.
- 514 Koch, D., and Del Genio, A. D.: Black carbon semi-direct effects on cloud cover: review and synthesis, *Atmos. Chem. Phys.*,
515 10, 7685-7696, 10.5194/acp-10-7685-2010, 2010.
- 516 Kompalli, S. K., Suresh Babu, S. N., Satheesh, S. K., Krishna Moorthy, K., Das, T., Boopathy, R., Liu, D., Darbyshire, E., Allan,
517 J. D., Brooks, J., Flynn, M. J., and Coe, H.: Seasonal contrast in size distributions and mixing state of black carbon and its
518 association with PM_{1.0} chemical composition from the eastern coast of India, *Atmos. Chem. Phys.*, 20, 3965-3985,
519 10.5194/acp-20-3965-2020, 2020.
- 520 Kuang, Y., He, Y., Xu, W., Yuan, B., Zhang, G., Ma, Z., Wu, C., Wang, C., Wang, S., Zhang, S., Tao, J., Ma, N., Su, H., Cheng, Y.,
521 Shao, M., and Sun, Y.: Photochemical Aqueous-Phase Reactions Induce Rapid Daytime Formation of Oxygenated Organic
522 Aerosol on the North China Plain, *Environmental science & technology*, 54, 3849-3860, 10.1021/acs.est.9b06836, 2020.
- 523 Lähde, T., Rönkkö, T., Happonen, M., Söderström, C., Virtanen, A., Solla, A., Kytö, M., Rothe, D., and Keskinen, J.: Effect of
524 Fuel Injection Pressure on a Heavy-Duty Diesel Engine Nonvolatile Particle Emission, *Environmental science & technology*,
525 45, 2504-2509, 10.1021/es103431p, 2011.
- 526 Li, Z., Tan, H., Zheng, J., Liu, L., Qin, Y., Wang, N., Li, F., Li, Y., Cai, M., Ma, Y., and Chan, C. K.: Light absorption properties
527 and potential sources of particulate brown carbon in the Pearl River Delta region of China, *Atmos. Chem. Phys.*, 19, 11669-
528 11685, 10.5194/acp-19-11669-2019, 2019.
- 529 Liu, D., Allan, J., Whitehead, J., Young, D., Flynn, M., Coe, H., McFiggans, G., Fleming, Z. L., and Bandy, B.: Ambient black
530 carbon particle hygroscopic properties controlled by mixing state and composition, *Atmospheric Chemistry and Physics*,
531 13, 2015-2029, 10.5194/acp-13-2015-2013, 2013.
- 532 Liu, D., Whitehead, J., Alfarra, M. R., Reyes-Villegas, E., Spracklen, D. V., Reddington, C. L., Kong, S., Williams, P. I., Ting, Y.-
533 C., Haslett, S., Taylor, J. W., Flynn, M. J., Morgan, W. T., McFiggans, G., Coe, H., and Allan, J. D.: Black-carbon absorption
534 enhancement in the atmosphere determined by particle mixing state, *Nature Geosci*, advance online publication,
535 10.1038/ngeo2901
536 <http://www.nature.com/ngeo/journal/vaop/ncurrent/abs/ngeo2901.html#supplementary-information>, 2017.
- 537 Liu, D., Joshi, R., Wang, J., Yu, C., Allan, J. D., Coe, H., Flynn, M. J., Xie, C., Lee, J., Squires, F., Kotthaus, S., Grimmond, S.,
538 Ge, X., Sun, Y., and Fu, P.: Contrasting physical properties of black carbon in urban Beijing between winter and summer,
539 *Atmos. Chem. Phys.*, 19, 6749-6769, 10.5194/acp-19-6749-2019, 2019.
- 540 Liu, J., Li, J., Zhang, Y., Liu, D., Ding, P., Shen, C., Shen, K., He, Q., Ding, X., Wang, X., Chen, D., Szidat, S., and Zhang, G.:
541 Source apportionment using radiocarbon and organic tracers for PM_{2.5} carbonaceous aerosols in Guangzhou, South



- 542 China: contrasting local- and regional-scale haze events, *Environmental science & technology*, 48, 12002-12011,
543 10.1021/es503102w, 2014.
- 544 Liu, L., Kuang, Y., Zhai, M., Xue, B., He, Y., Tao, J., Luo, B., Xu, W., Tao, J., Yin, C., Li, F., Xu, H., Deng, T., Deng, X., Tan, H., and
545 Shao, M.: Strong light scattering of highly oxygenated organic aerosols impacts significantly on visibility degradation,
546 *Atmos. Chem. Phys.*, 22, 7713-7726, 10.5194/acp-22-7713-2022, 2022.
- 547 Lu, T., Cheung, C. S., and Huang, Z.: Size-Resolved Volatility, Morphology, Nanostructure, and Oxidation Characteristics of
548 Diesel Particulate, *Energy & Fuels*, 26, 6168-6176, 10.1021/ef3010527, 2012.
- 549 Luo, B., Kuang, Y., Huang, S., Song, Q., Hu, W., Li, W., Peng, Y., Chen, D., Yue, D., Yuan, B., and Shao, M.: Parameterizations
550 of size distribution and refractive index of biomass burning organic aerosol with black carbon content, *Atmos. Chem. Phys.*,
551 22, 12401-12415, 10.5194/acp-22-12401-2022, 2022.
- 552 Man, R., Wu, Z., Zong, T., Voliotis, A., Qiu, Y., Groß, J., van Pinxteren, D., Zeng, L., Herrmann, H., Wiedensohler, A., and Hu,
553 M.: Impact of water uptake and mixing state on submicron particle deposition in the human respiratory tract (HRT) based
554 on explicit hygroscopicity measurements at HRT-like conditions, *Atmos. Chem. Phys.*, 22, 12387-12399, 10.5194/acp-22-
555 12387-2022, 2022.
- 556 Menon, S., Hansen, J., Nazarenko, L., and Luo, Y.: Climate Effects of Black Carbon Aerosols in China and India, *Science*, 297,
557 2250-2253, doi:10.1126/science.1075159, 2002.
- 558 Middlebrook, A. M., Bahreini, R., Jimenez, J. L., and Canagaratna, M. R.: Evaluation of Composition-Dependent Collection
559 Efficiencies for the Aerodyne Aerosol Mass Spectrometer using Field Data, *Aerosol Science and Technology*, 46, 258-271,
560 10.1080/02786826.2011.620041, 2012.
- 561 Moteki, N., and Kondo, Y.: Effects of Mixing State on Black Carbon Measurements by Laser-Induced Incandescence,
562 *Aerosol Science and Technology*, 41, 398-417, 10.1080/02786820701199728, 2007.
- 563 Motos, G., Schmale, J., Corbin, J. C., Modini, R. L., Karlen, N., Bertò, M., Baltensperger, U., and Gysel-Beer, M.: Cloud
564 droplet activation properties and scavenged fraction of black carbon in liquid-phase clouds at the high-alpine research
565 station Jungfraujoch (3580 m a.s.l.), *Atmos. Chem. Phys.*, 19, 3833-3855, 10.5194/acp-19-3833-2019,
566 2019.
- 567 Ng, N. L., Herndon, S. C., Trimborn, A., Canagaratna, M. R., Croteau, P. L., Onasch, T. B., Sueper, D., Worsnop, D. R., Zhang,
568 Q., Sun, Y. L., and Jayne, J. T.: An Aerosol Chemical Speciation Monitor (ACSM) for Routine Monitoring of the Composition
569 and Mass Concentrations of Ambient Aerosol, *Aerosol Science and Technology*, 45, 780-794, Pii 934555189
570 10.1080/02786826.2011.560211, 2011.
- 571 Nichols, J. L., Owens, E. O., Dutton, S. J., and Luben, T. J.: Systematic review of the effects of black carbon on cardiovascular
572 disease among individuals with pre-existing disease, *International Journal of Public Health*, 58, 707-724, 10.1007/s00038-
573 013-0492-z, 2013.
- 574 Ning, Z., Chan, K. L., Wong, K. C., Westerdahl, D., Močnik, G., Zhou, J. H., and Cheung, C. S.: Black carbon mass size
575 distributions of diesel exhaust and urban aerosols measured using differential mobility analyzer in tandem with
576 Aethalometer, *Atmospheric Environment*, 80, 31-40, <https://doi.org/10.1016/j.atmosenv.2013.07.037>, 2013.
- 577 Peng, J., Hu, M., Guo, S., Du, Z., Zheng, J., Shang, D., Levy Zamora, M., Zeng, L., Shao, M., Wu, Y.-S., Zheng, J., Wang, Y.,
578 Glen, C. R., Collins, D. R., Molina, M. J., and Zhang, R.: Markedly enhanced absorption and direct radiative forcing of black
579 carbon under polluted urban environments, *Proceedings of the National Academy of Sciences*, 10.1073/pnas.1602310113,
580 2016.
- 581 Raatikainen, T., Brus, D., Hooda, R. K., Hyvärinen, A. P., Asmi, E., Sharma, V. P., Arola, A., and Lihavainen, H.: Size-selected
582 black carbon mass distributions and mixing state in polluted and clean environments of northern India, *Atmos. Chem.*
583 *Phys.*, 17, 371-383, 10.5194/acp-17-371-2017, 2017.
- 584 Ren, J., Zhang, F., Wang, Y., Collins, D., Fan, X., Jin, X., Xu, W., Sun, Y., Cribb, M., and Li, Z.: Using different assumptions of
585 aerosol mixing state and chemical composition to predict CCN concentrations based on field measurements in urban



- 586 Beijing, *Atmos. Chem. Phys.*, **18**, 6907-6921, 10.5194/acp-18-6907-2018, 2018.
- 587 Saleh, R., Robinson, E. S., Tkacik, D. S., Ahern, A. T., Liu, S., Aiken, A. C., Sullivan, R. C., Presto, A. A., Dubey, M. K., Yokelson,
588 R. J., Donahue, N. M., and Robinson, A. L.: Brownness of organics in aerosols from biomass burning linked to their black
589 carbon content, *Nature Geoscience*, **7**, 647, 10.1038/ngeo2220
590 <https://www.nature.com/articles/ngeo2220#supplementary-information>, 2014.
- 591 Saleh, R.: From Measurements to Models: Toward Accurate Representation of Brown Carbon in Climate Calculations,
592 *Current Pollution Reports*, 10.1007/s40726-020-00139-3, 2020.
- 593 Sarangi, B., Ramachandran, S., Rajesh, T. A., and Dhaker, V. K.: Characteristics of black carbon aerosol mixing state over an
594 urban region deduced using single particle soot photometer (SP2) and differential mobility analyzer (DMA), *Atmospheric
595 Pollution Research*, **11**, 574-582, <https://doi.org/10.1016/j.apr.2019.12.006>, 2020.
- 596 Schwarz, J. P., Gao, R. S., Fahey, D. W., Thomson, D. S., Watts, L. A., Wilson, J. C., Reeves, J. M., Darbeheshti, M.,
597 Baumgardner, D. G., Kok, G. L., Chung, S. H., Schulz, M., Hendricks, J., Lauer, A., Kärcher, B., Slowik, J. G., Rosenlof, K. H.,
598 Thompson, T. L., Langford, A. O., Loewenstein, M., and Aikin, K. C.: Single-particle measurements of midlatitude black
599 carbon and light-scattering aerosols from the boundary layer to the lower stratosphere, *Journal of Geophysical Research:
600 Atmospheres*, **111**, D16207, 10.1029/2006JD007076, 2006.
- 601 Sedlacek Iii, A. J., Lewis, E. R., Kleinman, L., Xu, J., and Zhang, Q.: Determination of and evidence for non-core-shell
602 structure of particles containing black carbon using the Single-Particle Soot Photometer (SP2), *Geophysical Research
603 Letters*, **39**, <https://doi.org/10.1029/2012GL050905>, 2012.
- 604 Seinfeld, J., and Pandis, S.: *Atmospheric Chemistry and Physics: From Air Pollution to Climate Change*, Third Edition, 2016.
- 605 Stabile, L., Fuoco, F. C., and Buonanno, G.: Characteristics of particles and black carbon emitted by combustion of incenses,
606 candles and anti-mosquito products, *Building and Environment*, **56**, 184-191,
607 <https://doi.org/10.1016/j.buildenv.2012.03.005>, 2012.
- 608 Sun, J. Y., Wu, C., Wu, D., Cheng, C., Li, M., Li, L., Deng, T., Yu, J. Z., Li, Y. J., Zhou, Q., Liang, Y., Sun, T., Song, L., Cheng, P.,
609 Yang, W., Pei, C., Chen, Y., Cen, Y., Nian, H., and Zhou, Z.: Amplification of black carbon light absorption induced by
610 atmospheric aging: temporal variation at seasonal and diel scales in urban Guangzhou, *Atmospheric Chemistry and
611 Physics*, **20**, 2445-2470, 10.5194/acp-20-2445-2020, 2020.
- 612 Tan, H., Liu, L., Fan, S., Li, F., Yin, Y., Cai, M., and Chan, P. W.: Aerosol optical properties and mixing state of black carbon in
613 the Pearl River Delta, China, *Atmospheric Environment*, **131**, 196-208, <https://doi.org/10.1016/j.atmosenv.2016.02.003>,
614 2016.
- 615 Tasoglou, A., Louvaris, E., Florou, K., Liangou, A., Karnezi, E., Kaltsonoudis, C., Wang, N., and Pandis, S. N.: Aerosol light
616 absorption and the role of extremely low volatility organic compounds, *Atmospheric Chemistry and Physics*, **20**, 11625-
617 11637, 10.5194/acp-20-11625-2020, 2020.
- 618 Wang, Y., Li, W., Huang, J., Liu, L., Pang, Y., He, C., Liu, F., Liu, D., Bi, L., Zhang, X., and Shi, Z.: Nonlinear Enhancement of
619 Radiative Absorption by Black Carbon in Response to Particle Mixing Structure, *Geophysical Research Letters*, **48**,
620 e2021GL096437, <https://doi.org/10.1029/2021GL096437>, 2021.
- 621 Wilcox, E. M., Thomas, R. M., Praveen, P. S., Pistone, K., Bender, F. A.-M., and Ramanathan, V.: Black carbon solar
622 absorption suppresses turbulence in the atmospheric boundary layer, *Proceedings of the National Academy of Sciences*,
623 **113**, 11794-11799, doi:10.1073/pnas.1525746113, 2016.
- 624 Wu, Y., Xia, Y., Huang, R., Deng, Z., Tian, P., Xia, X., and Zhang, R.: A study of the morphology and effective density of
625 externally mixed black carbon aerosols in ambient air using a size-resolved single-particle soot photometer (SP2), *Atmos.
626 Meas. Tech.*, **12**, 4347-4359, 10.5194/amt-12-4347-2019, 2019.
- 627 Xu, Z., Li, X., Guan, C., and Huang, Z.: Effects of injection timing on exhaust particle size and nanostructure on a diesel
628 engine at different loads, *Journal of Aerosol Science*, **76**, 28-38, <https://doi.org/10.1016/j.jaerosci.2014.05.002>, 2014.
- 629 Yu, C., Liu, D., Hu, K., Tian, P., Wu, Y., Zhao, D., Wu, H., Hu, D., Guo, W., Li, Q., Huang, M., Ding, D., and Allan, J. D.:



630 Aerodynamic size-resolved composition and cloud condensation nuclei properties of aerosols in a Beijing suburban region,
631 *Atmos. Chem. Phys.*, 22, 4375-4391, 10.5194/acp-22-4375-2022, 2022.

632 Zhai, J., Yang, X., Li, L., Bai, B., Liu, P., Huang, Y., Fu, T.-M., Zhu, L., Zeng, Z., Tao, S., Lu, X., Ye, X., Wang, X., Wang, L., and
633 Chen, J.: Absorption Enhancement of Black Carbon Aerosols Constrained by Mixing-State Heterogeneity, *Environmental
634 science & technology*, 56, 1586-1593, 10.1021/acs.est.1c06180, 2022a.

635 Zhai, M., Kuang, Y., Liu, L., He, Y., Luo, B., Xu, W., Tao, J., Zou, Y., Li, F., Yin, C., Li, C., Xu, H., and Deng, X.: Insights into
636 characteristics and formation mechanisms of secondary organic aerosols in Guangzhou urban area, *Atmos. Chem. Phys.
637 Discuss.*, 2022, 1-29, 10.5194/acp-2022-807, 2022b.

638 Zhang, F., Wang, Y., Peng, J., Chen, L., Sun, Y., Duan, L., Ge, X., Li, Y., Zhao, J., Liu, C., Zhang, X., Zhang, G., Pan, Y., Wang, Y.,
639 Zhang, A. L., Ji, Y., Wang, G., Hu, M., Molina, M. J., and Zhang, R.: An unexpected catalyst dominates formation and
640 radiative forcing of regional haze, *Proceedings of the National Academy of Sciences*, 201919343,
641 10.1073/pnas.1919343117, 2020a.

642 Zhang, G., Lin, Q., Peng, L., Bi, X., Chen, D., Li, M., Li, L., Brechtel, F. J., Chen, J., Yan, W., Wang, X., Peng, P., and Sheng, G.,
643 and Zhou, Z.: The single-particle mixing state and cloud scavenging of black carbon: a case study at a high-
644 altitude mountain site in southern China, *Atmospheric Chemistry and Physics*, 17, 14975-14985, 10.5194/acp-17-14975-
645 2017, 2017.

646 Zhang, G., Fu, Y., Peng, X., Sun, W., Shi, Z., Song, W., Hu, W., Chen, D., Lian, X., Li, L., Tang, M., Wang, X., and Bi, X.: Black
647 Carbon Involved Photochemistry Enhances the Formation of Sulfate in the Ambient Atmosphere: Evidence From In Situ
648 Individual Particle Investigation, *Journal of Geophysical Research: Atmospheres*, 126, e2021JD035226,
649 <https://doi.org/10.1029/2021JD035226>, 2021.

650 Zhang, R., Khalizov, A., Wang, L., Hu, M., and Xu, W.: Nucleation and growth of nanoparticles in the atmosphere, *Chem
651 Rev*, 112, 1957-2011, 10.1021/cr2001756, 2012.

652 Zhang, Y., Zhang, Q., Cheng, Y., Su, H., Kecorius, S., Wang, Z., Wu, Z., Hu, M., Zhu, T., Wiedensohler, A., and He, K.:
653 Measuring the morphology and density of internally mixed black carbon with SP2 and VTDMA: new insight into the
654 absorption enhancement of black carbon in the atmosphere, *Atmospheric Measurement Techniques*, 9, 1833-1843,
655 10.5194/amt-9-1833-2016, 2016.

656 Zhang, Y., Favez, O., Canonaco, F., Liu, D., Močnik, G., Amodeo, T., Sciare, J., Prévôt, A. S. H., Gros, V., and Albinet, A.:
657 Evidence of major secondary organic aerosol contribution to lensing effect black carbon absorption enhancement, *npj
658 Climate and Atmospheric Science*, 1, 47, 10.1038/s41612-018-0056-2, 2018a.

659 Zhang, Y., Su, H., Ma, N., Li, G., Kecorius, S., Wang, Z., Hu, M., Zhu, T., He, K., Wiedensohler, A., Zhang, Q., and Cheng, Y.:
660 Sizing of Ambient Particles From a Single-Particle Soot Photometer Measurement to Retrieve Mixing State of Black Carbon
661 at a Regional Site of the North China Plain, *Journal of Geophysical Research: Atmospheres*, 123, 7778-7795,
662 <https://doi.org/10.1029/2018JD028810>, 2018b.

663 Zhang, Y., Zhang, Q., Yao, Z., and Li, H.: Particle Size and Mixing State of Freshly Emitted Black Carbon from Different
664 Combustion Sources in China, *Environmental science & technology*, 54, 7766-7774, 10.1021/acs.est.9b07373, 2020b.

665 Zhao, G., Tao, J., Kuang, Y., Shen, C., Yu, Y., and Zhao, C.: Role of black carbon mass size distribution in the direct aerosol
666 radiative forcing, *Atmos. Chem. Phys.*, 19, 13175-13188, 10.5194/acp-19-13175-2019, 2019.

667 Zhao, G., Li, F., and Zhao, C.: Determination of the refractive index of ambient aerosols, *Atmospheric Environment*, 240,
668 117800, <https://doi.org/10.1016/j.atmosenv.2020.117800>, 2020a.

669 Zhao, G., Shen, C., and Zhao, C.: Technical note: Mismeasurement of the core-shell structure of black carbon-containing
670 ambient aerosols by SP2 measurements, *Atmospheric Environment*, 243, 117885,
671 <https://doi.org/10.1016/j.atmosenv.2020.117885>, 2020b.

672 Zhao, G., Tan, T., Zhu, Y., Hu, M., and Zhao, C.: Method to quantify black carbon aerosol light absorption enhancement
673 with a mixing state index, *Atmos. Chem. Phys.*, 21, 18055-18063, 10.5194/acp-21-18055-2021, 2021.